Microelectromechanical system-based biocompatible artificial skin phantoms

Chien-Hao Liu[1] ✉, *Yin-Chen Huang*[2], *Shang-Hsuan Li*[1], *Yen-An Chen*[1], *Wesley Z Wang*[3], *Jia-Shing Yu*[4], *Wen-Pin Shih*[1]

[1]*Department of Mechanical Engineering, National Taiwan University, Taipei, Taiwan*
[2]*Institute of Applied Mechanics, National Taiwan University, Taipei, Taiwan*
[3]*Taipei American School, Taipei, Taiwan*
[4]*Department of Chemical Engineering, National Taiwan University, Taipei, Taiwan*
✉ *E-mail: cliu82@ntu.edu.tw*

Published in Micro & Nano Letters; Received on 30th April 2018; Revised on 23rd August 2018; Accepted on 5th December 2018

Revealing the physical interactions between biomedical devices and human skin requires a scalable phantom with physical properties as close as possible to those of human skin. In this work, the authors developed an artificial phantom for the simulation of human skin. The proposed device comprises a gelatin membrane, a layer of SU-8 photoresist, and microholes, respectively, mimicking the epidermis, stratum corneum, and sweat pores/ducts. A prototype was fabricated using microelectromechanical system and laser ablation techniques. The proposed structure includes microholes with a diameter of 20 μm and a depth of 57 μm distributed at a surface density of 620/cm^2 to simulate pores and sweat ducts. The mechanical and electrical properties of the fabricated phantom were compared with those of human skin. The electrical properties, such as resistivity and impedance, can be adjusted simply by varying the content of sodium chloride. 3T3 cells cultivated on the artificial phantom demonstrate their biocompatibility. The authors believe that the proposed phantom model and associated manufacturing scheme could be used to facilitate the testing of wearable and attachable bioelectronic devices.

1. Introduction: Artificial structures are attracting considerable attention for use in organ transplants, in vitro testing [1], and fundamental biomedical research, such as engineered vocal cords and three-dimensional (3D) printed devices including ears and hearts. Electrotherapy is a low-cost, non-invasive technique for medical treatments and pain relief; however, it is limited by the need for in vivo examinations and extensive clinical testing. In some cases, the application of excessive electricity can actually cause patients irreversible damage [2].

These shortcomings have led to the development of artificial skin phantoms to mimic human skin. Artificial skin phantoms are defined as engineering materials having similar physical and biological properties of real skin acting as counterparts of real skin which is also known as skin models or skin equivalents depending on different fields [3]. Artificial skin phantoms can be categorised as physical skin phantoms and tissue-engineered skin models. The former is used to mimic the physical characteristics of human skin for in vitro experiments, whereas the latter focuses on biological characteristics [3]. A gelatin-based model was developed to mimic the mechanical characteristics of human skin under the effects of injections. A silicone-based model doped with graphite was developed to simulate the electrical characteristics of human skin [4]. Tissue-engineered models provide a convenient system for in vitro biological research, particularly in the fields of drug delivery, wound healing, skin reconstruction, and a non-invasive instrument for skin-lesion evaluations [5]. They can also be used as an alternative to experimenting on animals.

In this research, we developed an artificial skin phantom that mimics both the physical and biological characteristics of human skin. The proposed structure comprises a gelatin membrane to simulate the epidermis, which is covered with a layer of SU-8 photoresist to simulate the stratum corneum of human skin. The characteristics of the proposed phantom are close to those of human skin in terms of geometric configuration as well as mechanical and electrical properties. Furthermore, microholes were fabricated on the surface of the phantom to simulate sweat ducts and pores. For different applications, we can change the electrical properties of the phantom by adding different quantities of sodium chloride (NaCl) into the phantom. 3T3 cells were also cultivated on the artificial phantom to evaluate its biocompatibility.

This Letter is organised as follows. The design and composition of the proposed artificial skin phantom are presented in the next section. We then describe the fabrication process with focus on the formation of surface microholes. This is followed by our experiments used to evaluate the mechanical and electrical properties of the phantom, as well as the cultivation of 3T3 cells on the surface of the device to determine its biocompatibility. Finally, we conclude with a summary of our results and their implications.

2. Design process

2.1. Geometric configuration: Human skin is a three-layer structure comprising the stratum corneum, epidermis, and dermis [6]. In our design of an artificial skin phantom, we replicated only the stratum corneum and epidermis (i.e. we disregarded the dermis) for two reasons. First, the respective resistivities (impedance) of the stratum corneum and epidermis exceed that of the dermis, such that the dermis has little effect on electrographic results [7]. Second, the dermis includes hair follicles, nerve endings, and blood vessels, the replication of which is beyond the objectives of this study. Thus, the proposed artificial skin phantom is a two-layer structure replicating the stratum corneum and epidermis. Human sweat contains several components such as moisture, sodium (Na^+), chloride (Cl^-) ions, lactic acid, disodium hydrogen phosphate, and L-histidine [8–11], which can affect the electrical properties. Therefore, we also sought to replicate sweat pores and sweat ducts in the proposed design.

Fig. 1*a* illustrates the geometric configuration of the proposed phantom comprising a gelatin membrane (thickness (h_1) of 70–100 μm) to simulate the epidermis and a layer of SU-8 photoresist (thickness (h_2) of 10–40 μm) to simulate the stratum corneum of human skin [7]. Small microholes were fabricated in the surface of the phantom to simulate sweat pores and ducts. The holes have a diameter (Φ) of 20–50 μm, length (h_3) of 100–900 μm, and spacing (d) of 350–700 μm. These values tend to vary according to the location on the human body [12].

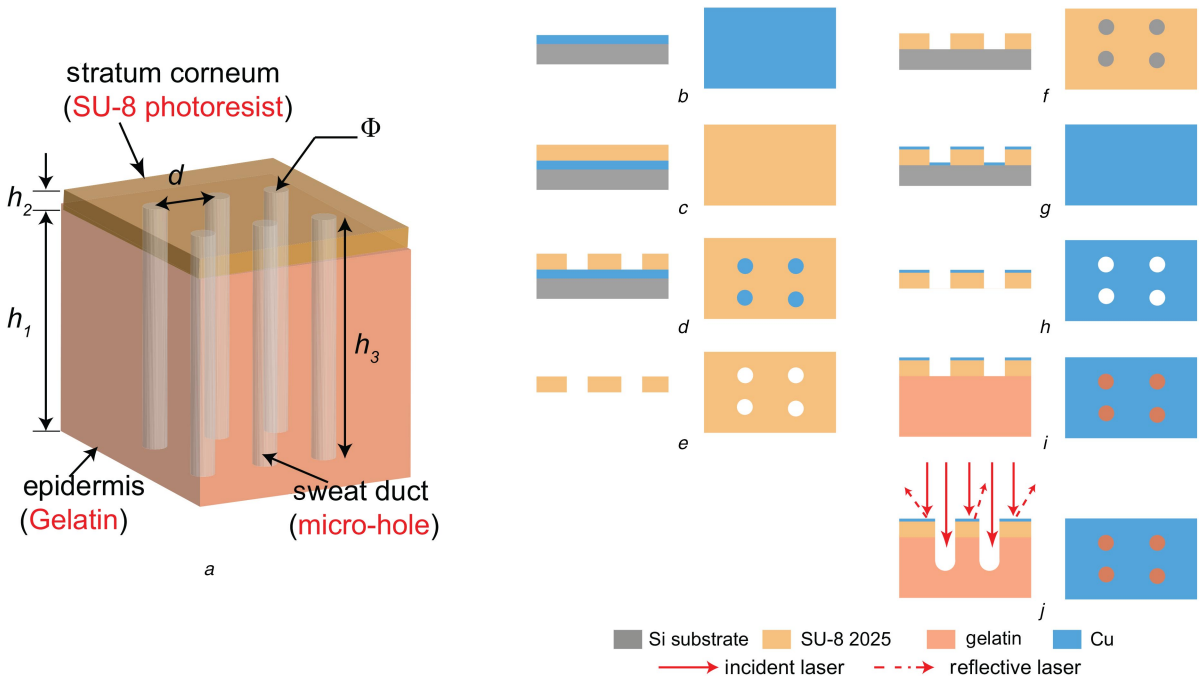

Fig. 1 *Illustration of our artificial skin phantom and its fabricaiton processes*
a 3D topology of proposed artificial skin phantom. Fabrication of proposed phantom
b Layer of copper deposited on four-inch silicon wafer
c Layer of SU-8 photoresist deposited over copper layer
d SU-8 photoresist patterned with numerous microholes using standard photolithographic techniques
e Lift-off processing used to pattern SU-8 photoresist by etching out sacrificial copper layer with etchant
f SU-8 photoresist mounted on a four-inch silicon wafer with tape
g Layer of copper deposited on photoresist
h Patterned SU-8 photoresist with copper coating removed from wafer
i SU-8 photoresist mounted on gelatin membrane via solidification
j laser ablation for creating microholes in surfaces of phantom and copper layers are then removed using copper etchant to obtain final phantoms (right and left columns are, respectively, cross-sections and top views

Table 1 Geometric parameters of proposed skin phantom (unit: μm)

h_1	h_2	h_3	d	Φ
70–100	10–40	100–900	350–700	20–50

Geometric parameters of the proposed phantom are listed in Table 1.

2.2. Composition: We selected SU-8 2025 photoresist to mimic the stratum corneum due to its high resistance to external electric stimulation, which is similar to that of the stratum corneum in actual skin [13]. Furthermore, the thickness of SU-8 photoresist is easily adjusted over a range of 10–40 μm (i.e. the thickness of the stratum corneum) [14]. The fact that SU-8 photoresist is a negative-tone photoresist also makes it easy to pattern microholes for the simulation of sweat pores using standard photolithographic techniques.

We selected gelatin to mimic the epidermis because gelatin is a natural material extracted from the skin, tendons, ligaments or bones of animals. Gelatin can be obtained by dissolving gelatin powders in hot water to produce an elastic solid through the formation of hydrogen bonds within the gelatin solution as it cools. The mechanical strength of gelatin can also be enhanced to more closely mimic the epidermis by initiating cross-linking reactions. Gelatin is naturally non-conductive; however, it can be made conductive by mixing conductive elements, such as acetic acid, graphene or lithium ion into the gelatin solution [15]. Furthermore, the electrical properties can be adjusted by altering the concentrations of charged particles. The biocompatibility of gelatin has also led to its wide application as a scaffold material for cell culturing. Some preliminary work was presented in [16].

3. Fabrication: The process of fabricating the proposed phantom can be divided into two parts. The SU-8 photoresist layer and the gelatin membrane are first fabricated using microelectromechanical system techniques, as shown in Figs. 1*b*–*i*. Microholes are then created in the surfaces of the phantom via laser ablation, as shown in Fig. 1*j*. Since the laser beam sizes of our laser equipment were larger than the desired sizes of microholes, the microholes were created in two stages. First, the microholes were generated on SU-8 via photolithography. After fabricating the SU-8 and gelatin, the laser ablation was exploited to fabricate microholes on gelatin and a Cu-based layer was used to block excessive laser.

3.1. Two-layer skin phantom: We first deposited a thin copper layer (thickness of 200 nm) on a four-inch silicon wafer to act as a sacrificial layer, as shown in Fig. 1*b*. A layer of SU-8, 2025 photoresist was then applied over the copper layer via spin-coating to a thickness of 25 μm, as shown in Fig. 1*c*. Pores were simulated by patterning the SU-8 photoresist layer with microholes using a one-mask photolithography method in which the mask defined the diameter and density of the holes, as shown in Fig. 1*d*. The patterned SU-8 photoresist was released by etching the sacrificial copper layer using etchant (lift-off processing), as shown in Fig. 1*e*. The resulting SU-8 photoresist was then attached to a four-inch silicon wafer using tape, as shown in Fig. 1*f*. A layer of copper was deposited over the photoresist, as shown in Fig. 1*g*. Finally, the

doi: 10.1049/mnl.2018.5112

structure comprising the SU-8 photoresist and copper layer was removed from the silicon wafer, as shown in Fig. 1*h*.

The next step involved mounting the SU-8 photoresist layer on the gelatin membrane, as shown in Fig. 1*i*. The gelatin membrane was produced by dissolving 0.75 g of gelatin powder in 20 ml deionised water. The electrical properties of this layer could be adjusted by altering the quantity of NaCl added to the solution (0, 0.1, and 0.3 g). The solutions were heated to 70°C and then subjected to mixing over a period of 5 h. After cooling, the gelatin solutions were placed separately in petri dishes with the SU-8 photoresist layers fabricated in the previous step as well as 50 µl of glutaraldehyde as a cross-linking agent. The gelatin solutions were solidified with the SU-8 photoresist layers over a period of two days. Glutaraldehyde is cytotoxic; therefore, we carefully controlled the quantity to prevent damage to tissue [17].

3.2. Microholes: The final step in the fabrication process involved the patterning of microholes in the surface of the skin phantom, as shown in Figs. 1*b*–*i*. This was achieved using the laser ablation technique illustrated in Fig. 1*j*. We employed an M-360 Laser Engraving and Cutting System to ablate the phantom. As shown in Fig. 1*j*, when the phantom was illuminated by the laser, the regions covered by the copper layer reflected the incident laser beams and in so doing protect the area beneath. As shown in Fig. 1*j*, the uncovered regions were exposed to the laser light, which causes the surface of the gelatin to heat up and partially vaporise when they reached temperatures exceeding the boiling point. This resulted in the formation of microholes on the surface of the gelatin membrane. The copper layer was then removed using a copper etchant to obtain the final skin phantoms shown in Fig. 1*j*.

The duration and power of ablation are the two main factors affecting the ablation depth. To create microholes of an appropriate depth, we formulated a heat transfer model to estimate the depth of ablation in the gelatin membrane, as shown in Fig. 2*a*. The gelatin membrane was assumed to be a 1D semi-infinite structure capable of absorbing all of the heat energy of the incident laser. Based on heat transfer theory [18], the governing equation can be expressed as follows:

$$\frac{\partial^2\theta}{\partial x^2} = \frac{1}{\alpha^*}\frac{\partial\theta}{\partial t} \quad 0 < x < \infty, \quad 0 < t, \tag{1}$$

where x indicates the direction of ablation and t indicates the ablation duration. $\theta(x, t)$ denotes the temperature difference between the gelatin membrane and room temperature. α^* is the modified thermal diffusivity of the gelatin to account for the influence of boiling. The convectional thermal diffusivity of gelatin, α, was defined as $\alpha = k/\rho c_p$, where k represents the thermal conductivity of gelatin, ρ is the density of the gelatin, and c_p is the specific heat capacity of the gelatin. α^* is defined [19] as

$$\alpha^* = \frac{k}{\rho c_p + (\text{latent heat}/\Delta T)}, \tag{2}$$

where ΔT indicates the temperature difference between the boiling point of the gelatin and room temperature. The initial condition is expressed as follows:

$$\theta(x, 0) = 0. \tag{3}$$

It was assumed that the laser source emitted a constant heat flux, the boundary condition of which is expressed as follows:

$$\theta(\infty, t) = \text{finite} - k\theta_x(0, t) = q, \tag{4}$$

where q is the heat flux per area of the incident laser beams.

The solution to these equations is expressed as

$$\theta(x, t) = \frac{q}{k}x\left[\text{erf}\left(\frac{x}{2\sqrt{\alpha^* t}}\right) + \frac{2e^{-(x^2/4\alpha^* t)}\sqrt{\alpha^* t}}{x\sqrt{(\pi)}} - 1\right]. \tag{5}$$

The solution indicating the temperature distribution as a function of ablation depth in the gelatin membrane is shown in Fig. 2*b*. We obtained the temperature distribution without considering the effects of boiling to substitute the conventional value of thermal diffusivity for the modified value of thermal diffusivity. As mentioned before, we determined the depth of the microholes when the temperature was below the boiling point. Under the practical ablation conditions encountered during fabrication (e.g. ablation time of 0.1 s and laser power of 25 W/mm^2), the estimated ablation depth ranged from 119 to 437 µm.

Fig. 3 presents the ablation depth under various incident power levels. The range of ablation depths is based on conventional and modified thermal diffusivity values, wherein the ablation depth increased with the power flux. This model can be used to determine the power flux associated with the ablation depth required for various applications. The proposed approach could be extended to other materials using laser illumination with arbitrary power levels.

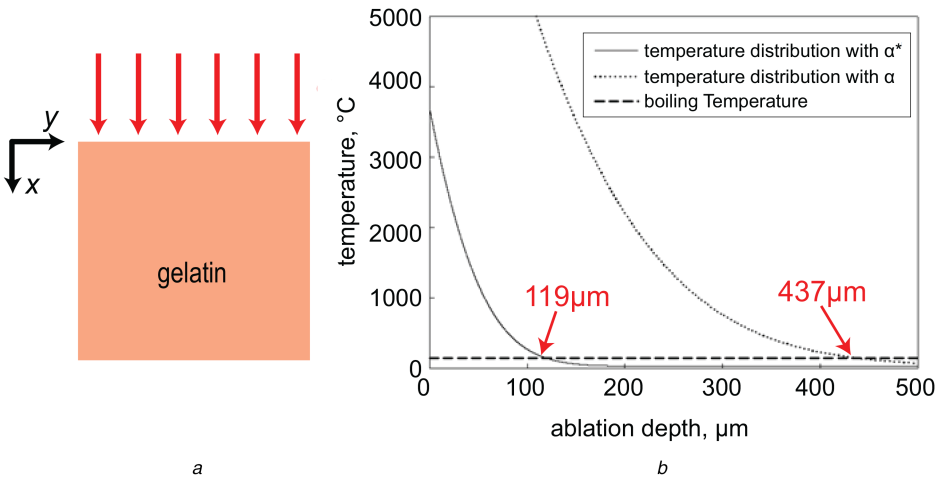

Fig. 2 *Illustration of the laser illumination processes for fabricating micro-holes on skin phantom*
a Proposed 1D semi-infinite heat transfer model of gelatin membrane under laser illumination at constant heat flux
b Temperature distribution as function of ablation depth based on conventional and modified thermal diffusivity: ablation applied for a duration of 0.1 s at laser power of 25 W/mm^2, which resulted in ablation depth ranging from 119 to 437 µm

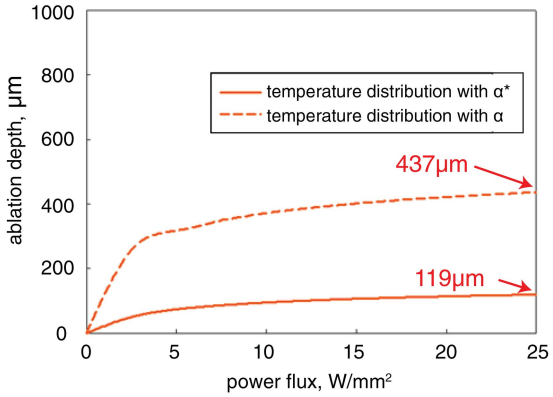

Fig. 3 *Estimated depth of ablation into gelatin membrane under various incident laser power levels (range of ablation depths based on conventional and modified thermal diffusivity)*

4. Experimental examination

4.1. Geometric configuration: Fig. 4*a* presents a photograph of the fabricated phantom. According to the film thickness gauge, the entire phantom (including SU-8 photoresist layer and gelatin membrane) was 115.6 ± 11.4 μm in thickness. Fig. 4*b* presents a top-view image of the phantom obtained using an optical microscope at 4× magnification. The array of black dots on the surfaces is the microholes simulating the pores and sweat ducts. The density of microholes was 620/cm^2 ± 8/cm^2. Fig. 4*c* presents a zoomed-in image of a microhole obtained using an optical microscope at 100× magnification, showing that the diameter of the microhole was 20 μm ± 3 μm. The vertical depth of the microhole was 57.2 ± 6.3 μm, as measured using the optical topography measurement instrument presented in Fig. 4*d*. The morphologic parameters of the phantom fell within the range of human skin, as shown in Table 1.

4.2. Mechanical properties: Fig. 5 presents the compression testing system comprising a load cell (LTS-A ultra-small capacity) and a precision motion platform for characterising the mechanical

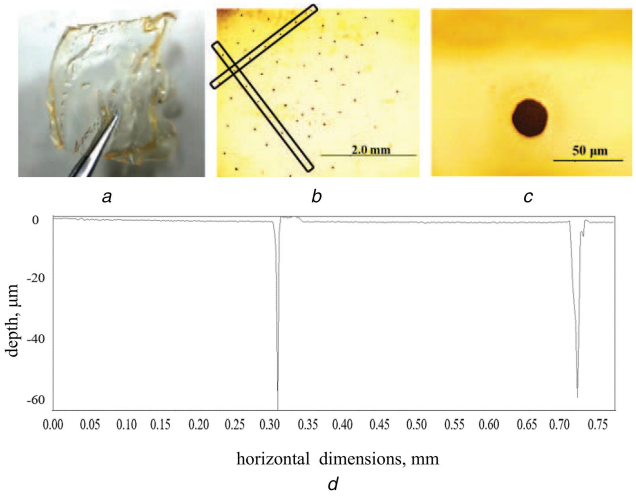

Fig. 4 *Geometric measurements of the fabricated skin phantom*
a Photograph of fabricated phantom
b Top-view image of phantom obtained using an optical microscope at 4× magnification (black dots are microholes simulating pores and sweat ducts
c Zoomed-in image of microhole obtained using an optical microscope at 100× magnification
d Cross-section profile of phantom measured using optical topography measurement instrument

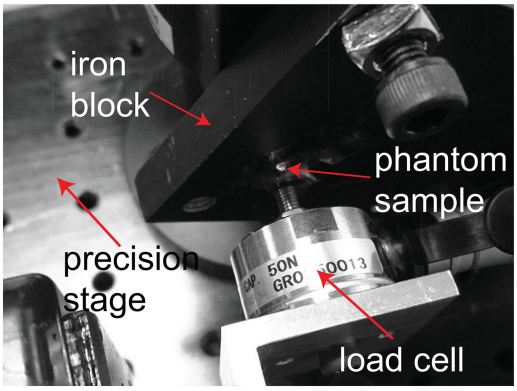

Fig. 5 *Experiment setup used to the characterise mechanical properties of fabricated phantom*

Table 2 Young's modulus of fabricated phantoms created using various concentrations of NaCl

Concentrations of NaCl, %	Young's modulus, MPa
0	1.6
0.5	1.1
1.4	1.7

properties of the fabricated phantoms. Three samples (30 mm×10 mm) were extracted from skin phantoms previously fabricated using three concentrations of NaCl. The samples were placed between the load cell and a fixed iron block. Based on the movement of the platform, the compressive deformation of the samples and the applied forces measured by the load cell were used to derive the Young's modulus of the sample. As shown in Table 2, the Young's moduli fell within the range of human skin (i.e. between 100 kPa and 20 MPa).

4.3. Electrical properties: Fig. 6*a* illustrates the experimental setup used to measure the electrical properties of the artificial skin phantoms produced using three different concentrations of NaCl. The samples were sandwiched between two parallel electrodes and maintained at precisely the same distance using a micrometre calliper. Impedance values, Z, were obtained by a calibrated impedance analyser (Agilent E4990a). Fig. 6 presents a photograph of the measurement system.

Since the measured impedance ($Z = R + jX$) depended on the size of the sample, we used only the real part to derive the resistivity of the phantom in order to remove the effect of dimensions, which can be expressed as

$$\rho_R = \frac{A}{h_1 + h_2} R, \tag{6}$$

where ρ_R is the resistivity and A is the area in cross section. h_1 and h_2 indicate the depths of the gelatin membrane and SU-8, respectively. The resistivity is inversely proportional to the combined length of the SU-8 and gelatin membrane (i.e. $h_1 + h_2$). The resistivity measurements of the three phantom samples are presented in Fig. 7. We observed a decrease in resistivity with an increase in frequency. The resistivity values fell within the range of human skin, i.e. ~10^7 Ωm at low frequency of 1 kHz and 10^4 Ωm and high frequency of 1 MHz [20].

This experiment demonstrated that the electrical properties of the proposed phantoms can be adjusted simply by altering the concentration of NaCl. This makes it possible to simulate skin in various regions of the human body. Fig. 8*a* presents the equivalent electrical

doi: 10.1049/mnl.2018.5112

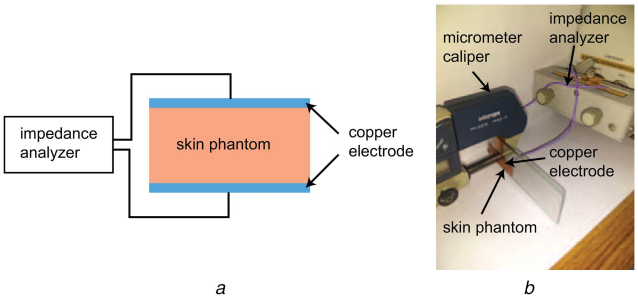

Fig. 6 *Electrical-property measurements of the fabricated skin phantom*
a Experiment setup used to characterise electrical properties of skin phantoms (calibrated impedance analyser used to measure impedance of samples sandwiched between two parallel electrodes)
b Photograph of the measurement system in which calliper is used to maintain copper electrodes at a precise distance

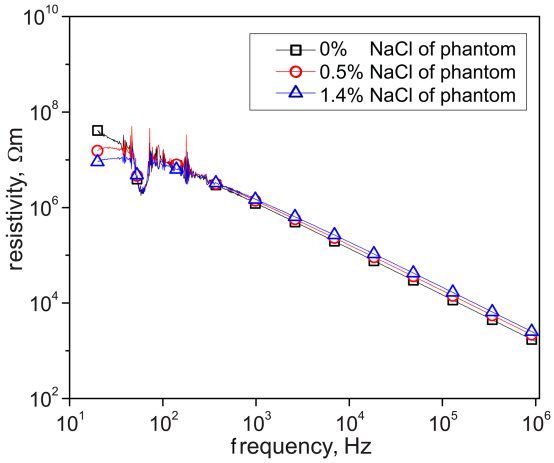

Fig. 7 *Measured resistivity as a function of frequency obtained from phantom samples produced using three different concentrations of NaCl (resistivity is shown to decrease with increase in frequency)*

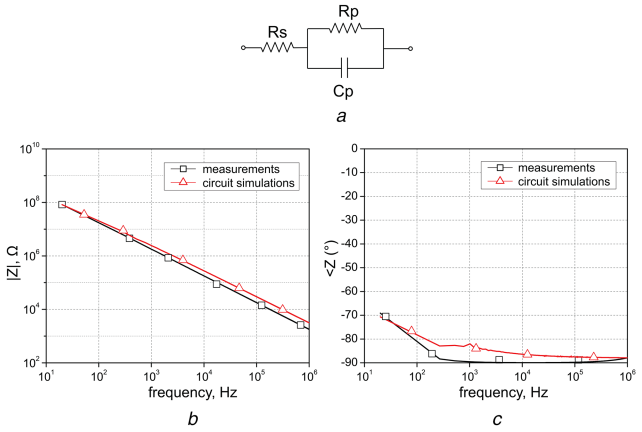

Fig. 8 *Electrical characterisations of the fabricated skin phantom*
a Equivalent electrical circuit model of proposed phantoms [21]
b Magnitude and phase of impedance values of the phantom, as derived from circuit simulations and measurements from samples produced without NaCl (extracted circuit parameters are shown in Table 3)

Table 3 Extracted circuit parameters of equivalent circuit model

R_s	650 Ω
R_p	234 M
C_p	89 pF

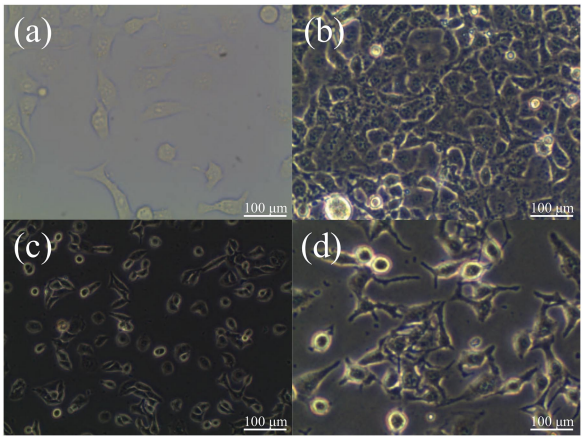

Fig. 9 *Photographs of 3T3 fibroblast cells cultivated in T-75 dishes containing a high-glucose medium, obtained using an inverted microscope: half of the 3T3 cells cultivated in a high-glucose medium for*
a 1 day
b 3 days; another half of the 3T3 cells cultivated on the surface of a gelatin membrane immersed in the high-glucose medium for
c 1 day
d 3 days

circuit model of the proposed phantoms, based on the equivalent circuit model of human skin reported in [22]. In this model, R_s refers to the resistance of deep tissue, and the parallel elements R_p and C_p refer to the impedance of the skin. Fig. 8*b* and *c* present the magnitude and phase of the impedance values of the phantom, as derived from circuit simulations and measurements of the sample produced without NaCl. The circuit parameters for the low-frequency applications presented in Table 3 were extracted via curve fitting. The fact that the phantoms demonstrate electrical behaviour similar to that of human skin [22] means that they could be used to estimate the electrical response of human skin in otherwise risky or harmful experiments.

4.4. Bio-compatibility: We examined the bio-compatibility of the fabricated phantoms by cultivating 3T3 fibroblast cells on them. SU-8 photoresist is a bio-compatible material and the gelatin membranes used to simulate the epidermis are the main components interacting with the targeted cells [23]. Thus, we only examined the bio-compatibility of the gelatin membrane. 3T3 fibroblast cells were first cultured in a T-75 dish under high glucose levels for one week and then separated into two T-75 dishes. Half of the 3T3 cells were cultivated in high-glucose medium in one of the dishes for 3 days as a control, as shown in Figs. 9*a* and *b*. The other half of the 3T3 cells were cultivated for three days on the surface of the fabricated gelatin membrane immersed in high-glucose medium, as shown Figs. 9*c* and *d*. Our results revealed that the 3T3 cells in both groups grew at similar rates, thereby confirming the bio-compatibility of the proposed phantoms.

5. Conclusions: In this research, we created an artificial skin phantom that mimics real human skin for use in scientific investigations. Unlike existing skin phantoms, the proposed phantom contains surface microholes to simulate pores and sweat ducts. A fabricated prototype presented mechanical properties, electrical properties, and bio-compatibility similar to those of human skin. The electrical properties of the skin phantom can also be adjusted simply by altering the concentration of NaCl. The proposed device is expected to be beneficial for the testing of wearable or attachable bioelectronic devices.

6. Acknowledgments: The authors would also like to thank the MEMS Research Center, National Taiwan University, Taiwan for granting access to their facilities. This work was supported by the Ministry of Science and Technology, Taiwan, under grant no. 104-2218-E002-033.

7 References

[1] Mao J., Zhao L., de Yao K., *ET AL.*: 'Study of novel chitosan-gelatin artificial skin in vitro', *J. Biomed. Mater. Res.*, 2003, **64A**, pp. 301–308

[2] Maruf F.A., Umunnah J.O., Akosile C.O.: 'Potential hazards and possible safety precautions in electrotherapy', *Afr. J. Physiother. Rehabil. Sci.*, 2013, **5**, pp. 8–15

[3] Grosse Perdekamp M., Pollak S., Thierauf A., *ET AL.*: 'Experimental simulation of reentry shots using a skin-gelatine composite model', *Int. J. Legal Med.*, 2009, **5**, pp. 419–425

[4] Akter F.: 'Tissue engineering made easy' (Elsevier Science, 2016)

[5] MacDonald M.: 'Your body: the missing manual' (O'Reilly Media, 2009, 1st edn)

[6] Martinsen O.G., Grimnes S.: 'Bioimpedance and bioelectricity basics' (Academic Press, 2008, 2nd edn.)

[7] Simpson B.A.: 'Electrical stimulation and the relief of pain' (Elsevier, Amsterdam, London, 2003, 1st edn.)

[8] Chen R., Qu J., Zhao Q., *ET AL.*: 'Environmental impact on the light and perspiration stability of triazinylstilbene fluorescent brighteners on cotton fabrics', *Fibers Polym.*, 2014, **15**, pp. 1915–1920

[9] Chen R., Qu J., Yang D., *ET AL.*: 'Light and perspiration stability of triazinylstilbene fluorescent brighteners on cotton fabrics', *Text. Res. J.*, 2014, **84**, pp. 772–782

[10] He H., Chen R., He J., *ET AL.*: 'The effects of L-histidine on the light and perspiration stability of 4,4′-diamino-stilbene-2,2′-disulfonic acid-based fluorescent whiteness agents on cotton fabrics', *Text. Res. J.*, 2015, **85**, pp. 775–782

[11] Zhang Y., Zhang X., Fang J., *ET AL.*: 'Application of SU-8 as the insulator toward a novel planar microelectrode array for extracellular neural recording'. IEEE 5th Int. Conf. on Nano/Micro Engineered and Molecular Systems, Xiamen, China, 2010, pp. 395–398

[12] Wilke K., Martin A., Terstegen L., *ET AL.*: 'A short history of sweat gland biology', *Int. J. Cosmet. Sci.*, 2007, **29**, pp. 169–179

[13] www.microchem.com

[14] Vieira D.F., Avellaneda C.O., Pawlicka A.: 'A short history of sweat gland biology', *Electrochim. Acta*, 2007, **29**, pp. 169–179

[15] Landi G., Sorrentino A., Iannace S., *ET AL.*: 'Electrical characterization and modeling of a gelatin/graphene system', *Adv. Condens. Matter Phys.*, 2015, **2015**, pp. 1–5

[16] Liu C.H., Chen Y.A., Yu J.S., *ET AL.*: 'Development of a gelatin-based artificial skin phantom for electrical treatments'. Second Association of Computational Mechanics Taiwan (ACMT) Conf., Taipei, Taiwan, 2016

[17] Allenby A.C., Fletcher J., Schock C., *ET AL.*: 'The effect of heat, pH and organic solvents on the electrical impedance and permeability of excised human skin', *Br. J. Dermatol.*, 1969, **81**, pp. 31–39

[18] Mitchell S.L., Myers T.G.: 'Heat balance integral method for one-dimensional finite ablation', *J. Thermophys. Heat Transf.*, 2008, **32**, pp. 508–514

[19] Machniewicz A., Heim D.: 'Modelling of latent heat storage in PCM modified components', *Czasopismo Techniczne*, 2015, **19**, pp. 161–167

[20] Warner R.R., Myers M.C., Taylor D.A.: 'Electron probe analysis of human skin: determination of the water concentration profile', *J. Invest. Dermatol.*, 1988, **90**, pp. 218–224

[21] Pieber K., Herceg M., Paternostro-Sluga T.: 'Electrotherapy for the treatment of painful diabetic peripheral neuropathy: a review', *J. Rehabil. Med.*, 2010, **42**, pp. 289–295

[22] Teixeira A.P., Rangel J.L., Raniero L.J., *ET AL.*: 'Confocal Raman spectroscopy: determination of natural moisturizing factor profile related to skin hydration', *Rev. Bras. Eng. Biomed.*, 2014, **30**, pp. 11–16

[23] Nemani K.V., Moodie K.L., Brennick J.B., *ET AL.*: 'In vitro and in vivo evaluation of SU-8 biocompatibility', *Mater. Sci. Eng. C, Mater. Biol. Appl.*, 2013, **33**, pp. 4453–4459

doi: 10.1049/mnl.2018.5112